Self-Stability Criteria and Verification of VSCs with Four AC-DC Coupled Droop Control Strategies

Yeji Jiang, Li "Lisa" Qi*, Jinzhuo Bai, Zhiguo Hao
School of Electrical Engineering
Xi'an Jiaotong University
Xi'an, China
jiangyeji@stu.xjtu.edu.cn, qili2024@xjtu.edu.cn

Abstract—**Droop control is a popular control strategy of DC microgrids because of achieving automated power distribution without communication among multiple converters. However, the self-stability of an AC-DC VSC equipped with different droop controls has not been fully examined. Thus, four droop controls, voltage-current (VI), voltage-power (VP), current-voltage (IV), power-voltage (PV) of the VSC based on the d-axis current or AC-DC coupled droop controls are studied in this paper. The self-stability evaluation criteria are deduced with physical meaning explained, providing some insights into the parameter selection in the VSC design. The effectiveness of the deduced self-stability criteria is verified by the simulation results of one example system. Further, the self-stability of the four droop controls is ranked from high to low and some recommendations are made on selecting proper droop controls.**

Keywords—DC microgrid, VSC, droop control, stability criteria, simulation verification.

I. INTRODUCTION

Recently, DC microgrids have more and more applications in many areas due to their advantages such as fewer power conversion stages, easiness of control [1] due to the absence of reactive power , simplified integration of renewable energy sources, and only voltage stability concerns compared to AC systems. The most popular control strategy to achieve power sharing among multiple voltage source converters (VSC) is droop control. Many researchers have already conducted research work in this area.

Comparative stability analysis of current-voltage (IV) and voltage-current (VI) droop controls based on the output current in VSC-based DC microgrids with constant power loads is studied in [2]. However, power-voltage (PV) and voltage-power (VP) droops are only partially considered. An AC–DC coupled droop control strategy for VSC-based DC Microgrids is proposed in [3] with the d-axis current reference i_{dref} directly calculated by $I_{\mathrm{d}}V$ control. Compared to the conventional IV droop control, the PI controller to derive i_{dref} is no longer needed. Thus, the output voltage response is able to achieve a smooth transition without any overshoot. The study in [3] mainly focuses on the stability analysis in the circumstance of a VSC with a IV droop loading by a constant power load via an RL line. The self-stability analysis of the VSC alone is neglected. Also, the other three droop controls, VI, VP, and PV, were not discussed. In [4], a comparative study of the four droop control strategies in buck-converter-based DC Microgrids is conducted, including the output current and the inductor current being the droop current, respectively. Almost all existing DC microgrid stability work focuses on converter interactions, assuming each converter being self-stable. Instead of the stability of converter interactions, this paper, adopting the coupled AC-DC coupled droop control, analyzes and evaluates the self-stability of a VSC with four droop control strategies. Further, self-stability evaluation criteria are deduced and verified. The main contributions in this paper are as follows:

- An equivalent circuit model generalized from the small-signal models of the four AC-DC coupled droop controls is derived.
- Based on the Routh–Hurwitz stability criterion, the time-constant-based and the load-current-based quantitative stability criteria of the four droops are proposed with physical meanings explained. These stability criteria provides some insights into the parameter selection in the design of self-stable VSCs.
- The self-stability of the four droops are ranked from best to worst with one example system at different operating conditions. In reality, the selection of appropriate droop controls should be a compromise between transient performance and stability considering working conditions.

This paper is arranged as follows. The small-signal models and a generalized equivalent circuit model of a VSC with the four AC-DC coupled droop control strategies are derived in section II. In section III, the stability criteria are deduced for each droop control. The effectiveness of the stability criteria are verified by simulation results in section IV with some suggestions on selecting appropriate droop controls. Finally, some conclusions and future work are presented in section V.

II. SMALL-SIGNAL MODELING OF VSCS WITH FOUR AC-DC COUPLED DROOP CONTROLS

Fig. 1 illustrates the topology and the control structure of the VSC studied in this paper. It is connected to the utility grid via an L-type filter. The grid impedance is neglected, as the focus of this study is on the DC-side stability of the VSC. For the inner-loop current control, the classical vector control in the *dq* frame is adopted. The *d*-axis current reference value i_{dref} is calculated by the outer-loop voltage control, i.e., the four droop control strategies, respectively. The six switching devices are driven by the inner-loop control outputs through Sinusoidal Pulse Width Modulation (SPWM).

A. Inner-Loop Control

According to the system topology and the inner-loop control structure shown in Fig. 1, with the state-space averaging method [5], the state-space averaging model in the *dq* frame of the VSC is able to be derived as

$$\begin{cases} v_{\mathrm{d}} = e_{\mathrm{d}} + \omega L_{\mathrm{f}} i_{\mathrm{q}} - \left(sL_{\mathrm{f}} + R_{\mathrm{f}}\right) i_{\mathrm{d}} \\ v_{\mathrm{q}} = e_{\mathrm{q}} - \omega L_{\mathrm{f}} i_{\mathrm{d}} - \left(sL_{\mathrm{f}} + R_{\mathrm{f}}\right) i_{\mathrm{q}} \end{cases} \tag{1}$$

This work was funded by the Key Research and Development Program of Shaanxi Province (No. 2024PT-ZCK-84).

XXX-X-XXXX-XXXX-X/XX/$XX.00 ©20XX IEEE
979-8-3315-8138-1

where ω is the nominal frequency of the grid in rad/s, e_d and e_q are the grid voltages at the point of common coupling (PCC), i_d and i_q are the currents through the L-type filter, v_d and v_q are the voltages of the VSC, R_f and L_f are the L-type filter resistance and inductance.

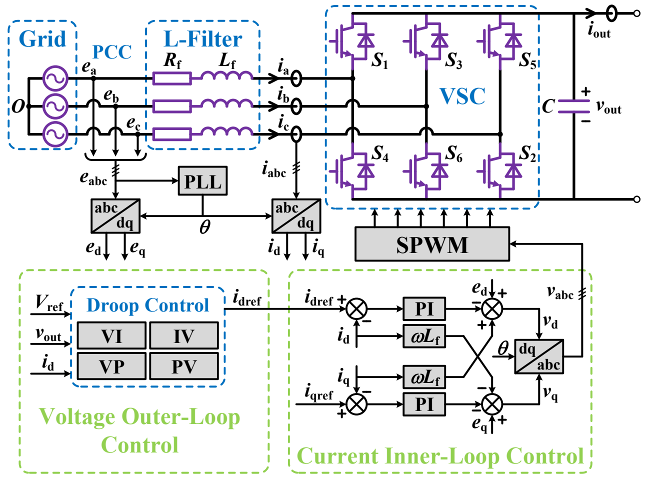

Fig. 1. The topology and the control structure of the VSC.

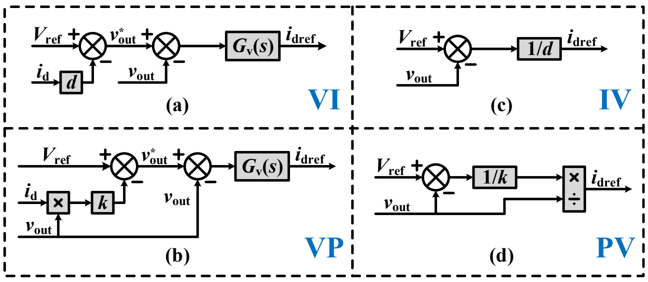

Fig. 2. Four AC-DC coupled droop control structures.

Under the dq-axis current decoupling control, the open-loop transfer function T_c of the inner-loop current control can be written as

$$T_c(s) = G_c \cdot \frac{1}{sL_f + R_f} = \frac{K_{pc} + K_{ic}/s}{sL_f + R_f} \tag{2}$$

where the first term G_c is the PI compensation control of the inner-loop current control, and the second term $1/(sL_f + R_f)$ is the controlled plant. K_{pc} and K_{ic} are the proportional and integral gains, respectively. The crossover frequency ω_c of T_c is approximately equal to K_{pc}/L_f since the values of K_{ic} and R_f are normally low.

Therefore, the closed-loop transfer function Φ_c of the inner-loop current control can be calculated as (3). It can be seen that in low-frequency range, Φ_c is approximately equal to 1, while in high-frequency range, Φ_c behaves as an integral element. For a unit negative feedback system, the bandwidth ω_b of Φ_c is approximately equal to the crossover frequency ω_c of T_c. Thus, Φ_c can be equivalently modeled as a first-order lag element with the bandwidth ω_c.

$$\Phi_c(s) = \frac{i_d(s)}{i_{dref}(s)} = \frac{T_c}{1+T_c} = \frac{G_c}{sL_f + R_f + G_c} \approx \frac{1}{s/\omega_c + 1} \tag{3}$$

Using the amplitude invariant transformation, the active power balance equation on both DC-side and AC-side and the capacitor charging and discharging equation are shown as (4). The state-space average model of the VSC system composed of (1) and (4), together.

$$\begin{cases} v_{out} i_{dc} = \frac{3}{2}\left(v_d i_d + v_q i_q\right) \\ sCv_{out} = i_{dc} - i_{out} \end{cases} \tag{4}$$

where C is the output capacitance. v_{out} is the output DC voltage. i_{dc} and i_{out} are the output currents before and after the capacitor respectively, as shown in Fig. 1.

In this paper, the d-axis is used to regulate the active power. Thus, e_d is the magnitude of the grid phase voltage, namely E_m, and e_q is equal to zero. To avoid consuming reactive power form the grid, the unity power factor control is adopted and thus the q-axis current reference value i_{qref} is set to zero. Each variable x in (1), (3), and (4) can be decomposed into a steady-state variable X and a small-signal variable Δx, i.e., $x = X + \Delta x$.

Therefore, the steady-state model of the VSC can be derived from (1) and (4) as shown in (5). The small-signal model of the VSC can be derived from (1), (3), and (4) as shown in (6).

$$\begin{cases} V_d = E_m - R_f I_d \\ V_{out} I_{out} = \frac{3}{2} V_d I_d \end{cases} \tag{5}$$

$$\begin{cases} \Delta v_d = \Delta e_d - \left(sL_f + R_f\right)\Delta i_d \\ \Delta i_d = \Phi_c \Delta i_{dref} \\ V_{out}\Delta i_{dc} + I_{out}\Delta v_{out} = \frac{3}{2}\left(V_d \Delta i_d + I_d \Delta v_d\right) \\ sC\Delta v_{out} = \Delta i_{dc} - \Delta i_{out} \end{cases} \tag{6}$$

Eliminating Δv_d, Δi_d, and Δi_{dc}, a small-signal model of the AC-DC VSC can be obtained from (6) as shown in (7), which only includes Δv_{out} , Δi_{out}, Δi_{dref} and Δe_d.

$$Y_c \Delta v_{out} + \Delta i_{out} = G_{VSC}\Delta i_{dref} + G_{ed}\Delta e_d \tag{7}$$

where the expressions for the coefficients of each variable are shown in (8). Y_c represents an equivalent output admittance of the VSC if i_{dref} is a constant, i.e., only controlled by the current-loop. G_{VSC} is the transfer function from Δi_{dref} to Δi_{out} if Δv_{out} is neglected. G_{ed} represents the d-axis voltage gain.

$$\begin{cases} Y_c(s) = sC + \frac{I_{out}}{V_{out}} = sC + \frac{1}{R_c} \\ G_{VSC}(s) = \frac{3}{2} \cdot \frac{V_d - I_d\left(R_f + sL_f\right)}{V_{out}} \cdot \Phi_c \\ G_{ed}(s) = \frac{3}{2} \cdot \frac{I_d}{V_{out}} \end{cases} \tag{8}$$

It is worth noting that G_{VSC} has a right-half-plane zero (RHPZ), leading to a negative regulation phenomenon (NRP). When the control signal increases, the output voltage exhibits a transient response where it initially decreases and then subsequently increases, and vice versa. The physical explanation is that when the control signal increases, the d-axis current takes time to increase to a new operating point, the load power must be temporarily supplied by the energy stored in the capacitor, resulting in a brief drop in the output voltage, and vice versa. This phenomenon, i.e., the RHPZ of G_{VSC} can pose some challenges to the converter stability, as investigated in section III.

B. Outer-Loop Control

The diagrams of the four AC-DC coupled droop control structures are illustrated in Fig. 2. The outer-loop voltage droop controls of VI, VP, IV, and PV directly derive the inner-loop current control references i_{dref} as (9), (10), (11), (12), respectively. G_v is equal to $K_{pv}+K_{iv}/s$. It is the PI compensation control of the outer-loop voltage controls of the VI and VP droop controls. K_{pv} and K_{iv} are the proportional and integral gains. To ensure an apple-to-apple comparison between VP/PV and VI/IV the four droops, k of the VP and PV droops is equal to d/V_{ref} to derive comparable steady-state values.

$$i_{dref} = G_v\left(v_{out}^{*} - v_{out}\right) = G_v\left(v_{ref} - d\cdot i_d - v_{out}\right) \tag{9}$$

$$i_{dref} = G_v\left(v_{out}^{*} - v_{out}\right) = G_v\left(v_{ref} - k\cdot i_d v_{out} - v_{out}\right) \tag{10}$$

$$i_{dref} = \frac{v_{ref} - v_{out}}{d} \tag{11}$$

$$i_{dref} = \frac{v_{ref} - v_{out}}{k\cdot v_{out}} \tag{12}$$

As can be seen in (5), the relationship between I_d and I_{out} is shown in (13). For the VI and IV droop controls based on the d-axis current, if the droop coefficient is d, their steady-state operating points are the same as the VI and IV droop controls based on the output current with the droop coefficient d/A. Likewise, the VP and PV droop controls have the same conclusions. Thus, although the product term $i_d v_{out}$ is a pseudo power and not equal to the output power of the VSC, the expressions of VP (10) and PV (12) are adopted in this paper.

$$\frac{I_{out}}{I_d} = \frac{3}{2}\cdot\frac{V_d}{V_{out}} \approx \frac{3}{2}\cdot\frac{E_m}{V_{ref}} = A \tag{13}$$

According to the outer-loop control equations (9)-(12), employing (3) to eliminate Δi_d, their small-signal models of the four droop controls can be generally derived as

$$\Delta i_{dref} = G_{vref}\Delta v_{ref} - G_{vout}\Delta v_{out} \tag{14}$$

where the expressions of G_{vref} and G_v are shown in TABLE I. K is equal to G_{vref}/G_v. For the VP droop and the PV droop, K is less than 1 but can be very close to 1 to derive (16).

TABLE I. EXPRESSIONS OF THE OUTER-LOOP CONTROL MODELS

	VI	VP	IV	PV
G_{vref}	$\frac{G_v}{1+dG_v\Phi_c}$	$\frac{G_v}{1+kV_{out}G_v\Phi_c}$	$\frac{1}{d}$	$\frac{1}{kV_{out}}$
G_{vout}	$\frac{G_v}{1+dG_v\Phi_c}$	$\frac{G_v\left(kI_d+1\right)}{1+kV_{out}G_v\Phi_c}$	$\frac{1}{d}$	$\frac{V_{ref}}{kV_{out}^2}$
K	1	$\frac{1}{kI_d+1}$	1	$\frac{V_{out}}{V_{ref}}$

C. Closed-Loop Transfer Functions

Plugging the small-signal models (14) of the four droop controls into (7), the small-signal model of the VSC system can be derived as a single equation as follows:

$$\left(Y_c + Y_v\right)\Delta v_{out} + \Delta i_{out} = KY_v\Delta v_{ref} + G_{ed}\Delta e_d \tag{15}$$

where Y_v is equal to $G_{VSC}G_{vout}$. Y_v represents an equivalent output admittance introduced by the outer-loop control G_{vout} and the inner-loop control G_{VSC}, together.

Therefore, the closed-loop transfer functions Φ_v from Δv_{ref} to Δv_{out} can be denoted as (16), where Z_v and Z_c are equal to $1/Y_v$ and $1/Y_c$, respectively. T_v is equal to Z_c/Z_v, which is the open-loop transfer function of the VSC system under unit negative feedback.

$$\Phi_v\left(s\right)\Big|_{\substack{\Delta e_d=0\\ \Delta i_{out}=0}} = \frac{\Delta v_{out}}{\Delta v_{ref}} = \frac{KY_v}{Y_c+Y_v} \approx \frac{Z_c}{Z_c+Z_v} = \frac{T_v}{1+T_v} \tag{16}$$

Likewise, the transfer functions G_{vv} from Δe_d to Δv_{out} can be denoted as (17). An equivalent output impedance Z_{out} considering the outer-loop controls can be written as (18).

$$G_{vv}\left(s\right)\Big|_{\substack{\Delta v_{ref}=0\\ \Delta i_{out}=0}} = \frac{\Delta v_{out}}{\Delta e_d} = \frac{G_{ed}}{Y_c+Y_v} \tag{17}$$

$$Z_{out}\left(s\right)\Big|_{\substack{\Delta v_{ref}=0\\ \Delta e_d=0}} = -\frac{\Delta v_{out}}{\Delta i_{out}} = \frac{1}{Y_c+Y_v} = \frac{1}{Y_{out}} \tag{18}$$

From (16) and (18), a generalized equivalent circuit of the four droop controls can be interpreted as shown in Fig. 3. It can be observed that the stability of the system depends on the interactions of the inner-loop and the outer-loop controls. From (8), R_c is an equivalent parallel resistor introduced by the inner-loop current control, and its value is equal to V_{out}/I_{out}.

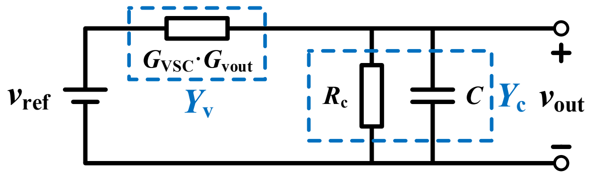

Fig. 3. A generalized equivalent circuit of the four droop controls.

III. SELF-STABILITY CRITERIA

In this section, the self-stability of the VSC under the four droop controls are analyzed and the stability evaluation criteria are deduced. The necessary and sufficient condition for system being stable is that the closed-loop transfer function has no right-half-plane pole (RHPP). The three transfer functions (16)-(18) have the same denominator. Therefore, the self-stability of the VSC can be analyzed by equalizing the same denominator to zero. Applying the deduction in (16), the characteristic equation of the VSC system divided by non-zero $G_{vout}\Phi_c$ is shown in (19). The second term $G_{VSC}/\ \Phi_c$ is a linear polynomial in s from (8).

$$1+T_v = 0 \quad\Rightarrow\quad \frac{Y_c}{G_{vout}\Phi_c} + \frac{G_{VSC}}{\Phi_c} = 0 \tag{19}$$

From TABLE I, the first term of (19) can be derived as a quadratic polynomial equation in s. Observing G_{VSC} in (8), the RHPZ mainly affects the system in high-frequency range, i.e., the NRP mainly occur in high-frequency range. In high-frequency range, for the VI and VP droop controls, the integrator element of the PI control in the outer-loop control is close to zero and can be neglected when analyzing (19). Based on this condition, for the VI and VP droop controls, the first term $Y_c/\ G_{vout}\Phi_c$ is also a quadratic polynomial in s. Therefore, (19) can be rewritten as (20). Moreover, only a_1

can be less than zero which is due to the RHPZ in G_{VSC}. The detailed deduction is skipped due to page limit.

$$a_0 s^2 + a_1 s + a_2 = 0 \tag{20}$$

According to the Routh–Hurwitz stability criterion [6], the necessary and sufficient condition to ensure the VSC system stability is that a_2, a_1, a_0 are all larger than zero. Thus, for (20), the system is stable as long as a_1 is larger than zero. Meanwhile, it also determines the damping of the system. It also can be seen in the simulation results in section IV.

A. VI Droop and VP droop

For the VI droop control, the expression of a_1 is derived as

$$a_1 = C\left(1 + dK_{\mathrm{pv}}\right) + \frac{1}{\omega_{\mathrm{c}} R_{\mathrm{c}}} - \frac{I_{\mathrm{out}} L_{\mathrm{f}} K_{\mathrm{pv}}}{V_{\mathrm{d}}} \tag{21}$$

Due to the high bandwidth ω_c of the inner-loop control, the term $1/\omega_c R_c$ can be omitted. Assuming that the parasitic resistance R_f of the L-type filter is sufficiently small, V_d is approximately equal to E_m. Thus, the time-constant-based and the load-current-based stability criteria of the VI droop control are derived as (22) and (23), respectively. D_d is equal to V_d/V_{out}, i.e., E_m/V_{out}.

$$\tau_{\mathrm{L}} = \frac{L_{\mathrm{f}}}{D_{\mathrm{d}}\left(d + \dfrac{1}{K_{\mathrm{pv}}}\right)} < R_{\mathrm{c}} C = \tau_{\mathrm{C}} \tag{22}$$

$$I_{\mathrm{out}} < \frac{E_{\mathrm{m}} C}{L_{\mathrm{f}}}\left(d + \frac{1}{K_{\mathrm{pv}}}\right) = I_{\max} \tag{23}$$

In (22), the left term τ_L and the right term τ_C represent the charging and discharging time-constants of the inductor and the capacitor, respectively. The physical meaning of this criterion is that the inductor must charge more rapidly than the capacitor discharges during the NRP, and vice versa.

For the VP droop control, replace d with kV_{out} in (22) and (23), the stability criteria of the VP droop control can be derived. Compared to the VI droop, the VP droop marginally degrades stability, because d is a bit larger than kV_{out}. In a word, the VP droop slows down the charging and discharging of the inductor. If this effect can be neglected, the stability criteria of the VP droop can also be denoted as (22), (23).

B. IV Droop and PV droop

For the IV droop control, the expression of a_1 is derived as

$$a_1 = C + \frac{1}{\omega_{\mathrm{c}} R_{\mathrm{c}}} - \frac{I_{\mathrm{out}} L_{\mathrm{f}}}{d V_{\mathrm{d}}} \tag{24}$$

With $1/\omega_c R_c$ neglected, the time-constant-based and the load-current-based stability criteria of the IV droop control are derived as (25) and (26), respectively. Compared to (22) and (23), they are similar in form. τ_L in (25) is larger than that in (22). Thus, the self-stability of IV is worse than VI.

$$\tau_{\mathrm{L}} = \frac{L_{\mathrm{f}}}{D_{\mathrm{d}} d} < R_{\mathrm{c}} C = \tau_{\mathrm{C}} \tag{25}$$

$$I_{\mathrm{out}} < \frac{E_{\mathrm{m}} C}{L_{\mathrm{f}}} d = I_{\max} \tag{26}$$

As in the analysis of the VI droop control, τ_L and τ_C of the IV droop in (25) represent the charging and discharging time-constants of the inductor and the capacitor.

For the PV droop control, the same method in the analysis of the VP droop can be applied. Compared to the IV droop control, the PV droop control marginally degrades stability. For simplification, the stability criteria of the PV droop control can also be denoted as (25), (26).

C. Stability Ranking of the Four Droop Controls

Applying the same VSC parameters, comparing (22)(23) and (25)(26), the stability of the VI/VP droops is better than the IV/PV droops. Adopting the VSC system parameters in TABLE II of section IV, the Nyquist plots of the VSC is plotted in Fig. 4. The stability margin of the four droop controls, ranking from the highest to the lowest, is VI, VP, IV, PV. It fully agrees with the theoretical analysis in this section.

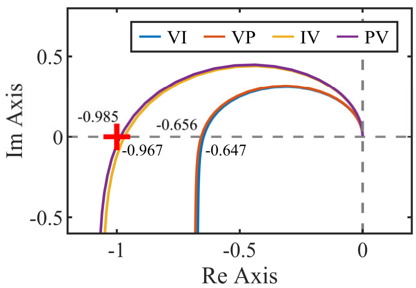

Fig. 4. The nyquist curves for the open-loop transfer functions T_v of the four droop controls in the system.

IV. SIMULATION VERIFICATION

In this section, using Matlab/Simulink/SPS, the stability criteria derived in section III are verified by time domain simulations. Meanwhile, the transient response of the output voltage of the four droop controls are also evaluated for the purpose of selecting proper droop control schemes. The parameters of the VSC in Fig. 1 are listed in TABLE II.

TABLE II. SIMULATION PARAMETERS OF THE VSC SYSTEM

E_m	V_{ref}	I_{out}	L_f	R_f	C	d
311 V	750 V	20 A	3 mH	0.06 Ω	1 mF	0.2
f_n	f_{sw}	K_{pc}	K_{ic}	K_{pv}	K_{iv}	k
50 Hz	48 kHz	90	2	10	1000	d/V_{ref}

A. Verification of Stability Criteria

For the four droop controls, the step changes of the load current, the two time-constants value calculated by (22) and (25), and the maximum load current value calculated by (23) and (26) are shown in Fig. 5. Obviously, the maximum load currents by the IV and PV are much lower than the VI and VP. Moreover, the output voltage response corresponding to the load current changes are illustrated in Fig. 5.

For the VI droop and the PV droop, if the load current is low, the output voltage exhibits overshoot without any oscillations and converges afterwards. With the load current increased, the output voltage exhibits extra oscillations, demonstrating a decrease in system damping. Compared to the VI droop control, the system damping of the VP droop control is smaller with the same load current. It is consistent with the analysis results in section III.A. If the load current exceeds the maximum allowable value, the output voltage exhibits oscillatory divergent instability. Meanwhile, τ_L is larger than

τ_C. Thus, the stability criteria (22) and (23) are validated by the simulation results.

For the IV droop and the PV droop, if the load current is low enough, the output voltage can achieve smooth transitions without any oscillations and overshoot. According to (20), with the load current increased, the system damping is decreasing, which is similar to what is observed from the VI droop and the VP droop. With the load current increased to sufficiently high values, the output voltage response exhibits overshoot, increased settling time, and oscillations before stabilizing at a new operating point. Compared to the IV droop control, the system damping of the PV droop control is a bit lower with the same load current. It is consistent with the analysis results in section III.B. If the load current exceeds the maximum allowable value, the output voltage exhibits oscillatory divergent instability. Meanwhile, τ_L become larger than τ_C. Thus, the stability criteria (25) and (26) are also validated by the simulation results.

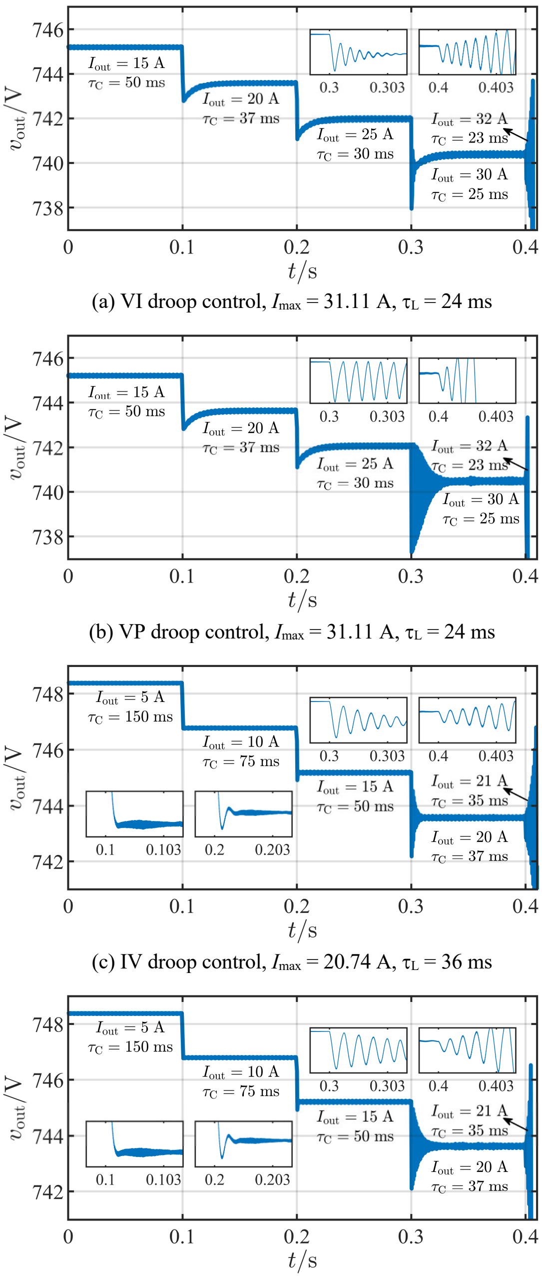

(a) VI droop control, I_{max} = 31.11 A, τ_L = 24 ms

(b) VP droop control, I_{max} = 31.11 A, τ_L = 24 ms

(c) IV droop control, I_{max} = 20.74 A, τ_L = 36 ms

(d) PV droop control, I_{max} = 20.74 A, τ_L = 36 ms

Fig. 5. The output voltage response curves of the four droop controls.

B. *Practical Concerns in Droop Control Selection*

The output voltage response of the four droop controls with the load current changing from 5 A to 10 A at 0.1 s is compared in Fig. 6. The VI and VP droops possess similar transitions with overshoot. However, the IV and PV droops can achieve similar fast and smooth transitions without overshoot. Therefore, if the load current is low, the IV and PV droops may be selected for faster and smoother transient response without stability violations. However, if the load current is high, the VI and VP droops are more recommended than the IV and PV droops due to higher stability margin.

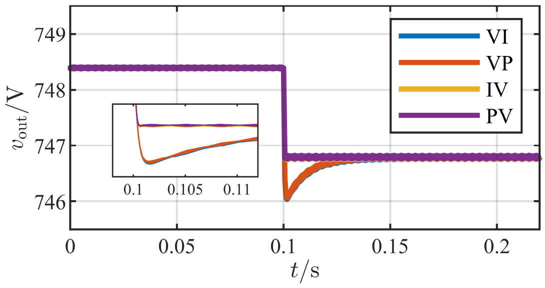

Fig. 6. The output voltage response comparison curves of the four controls.

V. CONCLUSIONS AND FUTURE WORK

This paper presents a self-stability analysis of the AC-DC coupled VI, VP, IV, and PV droop controls implemented on a VSC used in the rectification mode. Under the assumptions of the current inner-loop control first-order approximation and neglecting the voltage outer-loop control integration term, the self-stability criteria of the VSC with the four droop controls are proposed based on the Routh-Hurwitz stability criterion. The accuracy of the proposed criteria is verified by the simulation results of one example VSC system. Despite the faster and smoother transients by the IV and PV droops than the VI and VP droops, the stability regions of the IV and PV droops are much smaller than the VI and VP droops. This paper is the first step on DC microgrid stability analysis and paves the foundation of designing stable DC microgrids. In the future, more parametric analysis and the relationship between self-stability and interactions will be studied.

REFERENCES

[1] T. Dragičević, X. Lu, J. C. Vasquez and J. M. Guerrero, "DC Microgrids—Part I: A Review of Control Strategies and Stabilization Techniques," in *IEEE Transactions on Power Electronics*, vol. 31, no. 7, pp. 4876-4891, July 2016.

[2] F. Gao *et al.*, "Comparative Stability Analysis of Droop Control Approaches in Voltage-Source-Converter-Based DC Microgrids," in *IEEE Transactions on Power Electronics*, vol. 32, no. 3, pp. 2395-2415, March 2017.

[3] B. Zhang, F. Gao, Y. Zhang, D. Liu and H. Tang, "An AC-DC Coupled Droop Control Strategy for VSC-Based DC Microgrids," in *IEEE Transactions on Power Electronics*, vol. 37, no. 6, pp. 6568-6584, June 2022.

[4] L. L. Qi, M. Gao and S. Faddel, "Comparative Study of Four Droop Control Strategies in Buck Converter Based DC Microgrid," in *IEEE Transactions on Industry Applications*, vol. 60, no. 4, pp. 5331-5343, July-Aug. 2024.

[5] Jian Sun, D. M. Mitchell, M. F. Greuel, P. T. Krein and R. M. Bass, "Averaged modeling of PWM converters operating in discontinuous conduction mode," in *IEEE Transactions on Power Electronics*, vol. 16, no. 4, pp. 482-492, July 2001.

[6] C. Chen, Linear System Theory and Design, 3rd ed. New York: Oxford Univ. Press, 1999.